21, rue d'Artois, F-75008 PARIS
http : //www.cigre.org

CIGRE US National Committee
2021 Grid of the Future Symposium

Forecasting Dynamic Line Rating with Spatial Variation Considerations

T. PHILLIPS, A. ABBOUD, B. STARKS, J. LEHMER, J. GENTLE
Idaho National Laboratory
USA

SUMMARY

Dynamic line rating (DLR) is a technology that allows the ampacity of an electrical conductor to be calculated using real-time or forecasted weather conditions. Historically, the ampacity of a conductor has been determined using a static line rating method which assumes conservative weather assumptions. Therefore, not only can DLR give a more accurate measurement of the true ampacity of a conductor, but it can also increase its ampacity during weather conditions with greater thermal mitigations. The two primary cooling factors in the ampacity calculations are wind speed and direction. In complex terrain, wind speed and direction can have large variations over short distances. Therefore, accurately identifying the limiting span of a transmission line requires high spatial resolution of the wind along its path. One solution is to install dense weather stations along their path, though this can become costly over long distances. Therefore, researchers have investigated the use of Computation Fluid Dynamic (CFD) simulations to accurately compute the wind field along the path of a transmission line and use these results to identify the limiting section of the conductor.

This work presents a case study that evaluates the coupling of CFD simulations and forecasted weather simulations using the High-Resolution Rapid Refresh (HRRR) model points over a 2-year span within a region in south eastern Idaho. The primary goal of the work is the evaluation of the number of HRRR model points used, i.e., weather stations, along the path of the line and the accuracy of the resulting DLR ampacity. This was done using 4, 10, 17, 26, and 35 HRRR model points along two transmission line paths. The results indicate that as the number of model points are increased, the DLR ampacity of the lines decrease, yet converge as more points are added and demonstrate little change with additional HRRR points. It is expected that these results can help transmission line operators identify the number of weather stations that must be installed when coupled with CFD simulations and DLR ampacity to ensure accurate ratings and safe operations.

KEYWORDS

Dynamic line rating, computational fluid dynamics, overhead transmission lines, fluid dynamics, general line ampacity state solver

Tylerphillips@inl.gov

1. INTRODUCTION

The ampacity of a transmission line is defined as the maximum amount of current the conductor can safely carry. If the conductor becomes too hot its thermal expansion can put the public in danger due to loss of power, ignition of fires, or excessive conductor sag between supporting structures. Furthermore, if extreme conductor temperatures are reached, annealing of the conductor is possible. Therefore, it is necessary for transmission line operators to employ their assets with regard to the most accurate conductor ampacity.

The common practice to calculate ampacity is with a Static Line Rating (SLR) method as described by the International Council on Large Electric Systems [1], the International Electrochemical Commission [2], or the Institute of Electrical and Electronics Engineers (IEEE) [3], [4]. When a SLR method is used the rated ampacity does not change over time. It is well known that the assumptions used to calculate the SLRs are generally conservative, as they assume low wind speed, high ambient temperature, and high solar irradiance. Therefore, a SLR method results in ampacity that generally underestimates the actual ampacity since the real-time weather conditions are more favorable than what is assumed, such as higher wind speed or lower ambient temperatures. Because of this, transmission line operators may rate lines seasonally to take advantage of cooler ambient temperature. However, even with the use of seasonally rated ampacity, transmission line capacity is often underutilized. Because of this, many researchers are investigating the use of DLR to determine the potential for additional ampacity based on real-time or forecasted conditions.

The adoption of DLR has been shown to increase penetration of distributed generation due to lower curtailment. The synergy between wind generation and DLR provides great benefits for the integration of wind power [5]-[8]. It also provides better network support during an outage and can defer upgrades to the transmission system. Increasing ampacity above static ratings using DLR is demonstrated using historical weather data in the US and the UK [9] as well as Canada [10], [11]. The use of forecasted weather data has been used in Ireland [12], in addition to the use of CFD simulations [13], [14]. In further studies, DLR has shown potential with day ahead planning [15], or as a way for easing congestion of lines [16], [17], and has been identified as a key transmission and distribution infrastructure solution by the U.S. Department of Energy [18], [19].

Using CFD simulations in a DLR methodology has several significant advantages over other methods. First, installation of dense weather reading instrumentation along the path of long transmission lines can be costly, whereas CFD simulations give spatial wind fields needed for accurate ampacity calculations. Second, a CFD approach can be more cost effective than directly monitoring conductor temperature or sag of lines to infer the ampacity. Furthermore, direct monitoring solutions often require a period of outage to install. Lastly, even if it is desired to use direct measurement devices or weather station data for determining ampacity, CFD results can be used to identify the limiting section of the line. If there is not a weather station located at that point it would be a desired location for placement of a direct measurement device.

It is a prime interest of this work to demonstrate the ampacity results of coupled CFD wind fields with varying spatial resolutions of wind station measurements. However, the number of wind stations along the path of transmission lines in the study area is not dense enough for such a study, as shown in Fig. 1(a). Therefore, this work employs model points from the HRRR forecast data along the path of the transmission lines. The HRRR model [20] is a convection-allowing forecast model that outputs meteorological variables. It was developed at the National Oceanic and Atmospheric Administration Earth System Research Laboratory and is run operationally at the National Center for Environmental Prediction. The accuracy of ampacity calculations using the HRRR model is shown in [13]. Furthermore, this work leverages the Idaho National Laboratory (INL) General Line Ampacity State Solver (GLASS) software for the ampacity calculations. Inputs to GLASS are the CFD simulation results, transmission line structure locations, and the HRRR forecast data. In short, GLASS uses the HRRR data to pull a CFD wind field and scales the results accordingly. It then calculates the ampacity at every midpoint

between transmission structures and returns the limiting ampacity of the line. The reader is referred to [15] and [16] for further details of the GLASS software.

Additionally, this work presents a case study that examines the coupling of CFD simulations and DLR using forecasted HRRR data over a 2-year period in a region in south eastern Idaho. The evaluation of ampacity ratings based on different spatial resolution of HRRR points along transmission paths is shown. The results indicate that increasing spatial resolution of HRRR points results in lower ampacity. However, it is demonstrated that as a higher number of points are used, the reduction of ampacity is minimized. This indicates that the resulting ampacity becomes independent of further addition of points along the transmission line path. These results may help indicate the density of weather stations that are needed to be used with coupled CFD and DLR to ensure that ampacity ratings are accurate and ensure safe operation.

The rest of the paper is formatted as follows; Section 2 introduces the case study region. Section 3 gives a brief mathematical background for the CFD simulations and displays the resulting wind flow fields over the region. Section 4 gives the ampacity calculation equations, and the ampacity results are given in Section 5. Finally, a discussion on key findings of the study and concluding remarks are given in Section 6 as well as funding for this work in Section 7.

2. CASE STUDY REGION

The geographic location for the case study conducted in this paper is in a region of south eastern Idaho on the Idaho National Laboratory (INL) desert. The region of interest extends 30 km in the east/west direction and 50 km in the north/south direction. The digital elevation d of the region has a spatial resolution of 30 meters. The elevation map of the area is shown in Fig. 1(a), where the region of interest used in the CFD simulations is depicted by the black square. The two transmission lines used in this study, called the east and west loop, are also shown. The east transmission loop contains 281 support structures, and the west loop has a total of 230. The location of the transmission structures was provided through INL engineering drawings. The HRRR points nearest to the weather stations in the region are depicted by black diamonds.

3. COMPUTATIONAL FLUID DYNAMIC SIMULATIONS

The CFD simulations used in this study are done using steady state Reynolds-averaged Navier-Stokes (RANS) equations. The time scale of weather patterns and conductor temperature changes are not rapid enough to require an unsteady RANS approach or a more accurate large-eddy simulation that are more computationally expensive [21]. The steady state RANS approach allows computation time to remain manageable. In complex terrain RANS equations may not be well suited in regions after crossing hills as the downstream regions can produce an over-prediction of the speed up ratio [22]. The WindSim CFD software [23] used in this study employs the RANS turbulence model, which has been validated in complex terrain [24], [25]. Furthermore, Greenwood et al. [26] demonstrate that RANS simulations are accurate when comparing measured weather data to mapping weather station data from extrapolated locations with lookup tables as done in this paper.

The CFD simulations used in this work were ran using WindSim 9.0 commercial software. The simulation domain was created by making an x-y mesh with uniform 30-meter resolution provided by the digital elevation data. In the vertical direction, non-uniform spacing is adopted to provide better resolution near the ground surface, thus providing more accurate wind speed and direction results where transmission lines reside. A 5-meter resolution is applied from the surface to a height of 50 meters. The resolution is increased to 10 meters up to a height of 100 meters, and a growing pseudo-logarithmic spacing is then applied up to 3500 meters. A 10 m/s boundary condition is applied at the boundary layer height; a prior study showed that the sensitivity to this boundary condition is minor when coupled with available weather data in resource assessment [27] and significantly lower ground speeds are to be expected in the model.

Due to the computational cost of the high resolution of these simulations, the region is split in a northern and southern domain. The overlap is 10 km, and no structures within 5 km of the boundary are used to avoid potential boundary condition issues of the flow field. The northern mesh of the region for the divisions is shown in Fig. 1(b) and the southern in (c). Each of the computational domains contain 40 million cells. The vertical spacing of the grid is shown in Fig. 1(d).

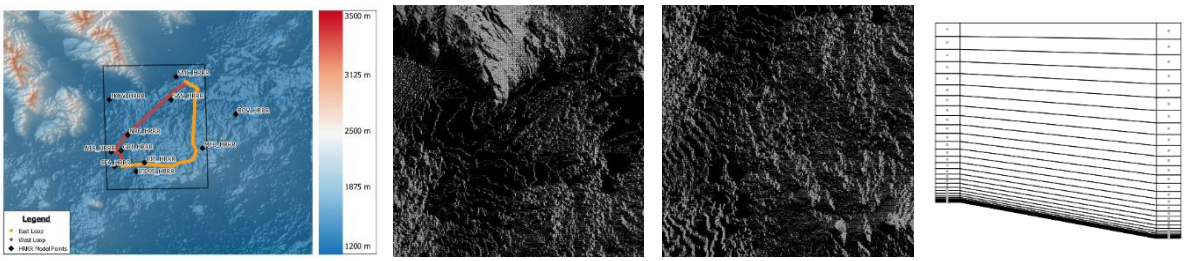

(a) (b) (c) (d)

Fig. 1. Terrain elevation map of INLs test site with east and west loop transmission lines, weather stations, and CFD domain. Horizontal mesh layout of northern (b), souther (c), and vertical (d) layout which shows the skewed mesh from high peaks to the low river elevation.

The partial differential equations dictating the wind field solution for the Reynolds-averaged Navier-Stokes (RANS) equations with the standard $k-\epsilon$ model that is used are the three velocity vectors, U_i, the turbulent kinetic energy, k, and the turbulent dissipation rate, ϵ. The RANS equations are given as follows

$$\rho U_i \frac{\partial U_j}{\partial x_i} = \frac{\partial}{\partial x_i}\left[(\mu + \mu_t)\left(\frac{\partial U_i}{\partial x_j} + \frac{\partial U_j}{\partial x_i}\right)\right] - \frac{\partial p}{\partial x_i} \tag{1}$$

$$\frac{\partial (U_i k)}{\partial x_i} = \frac{\partial}{\partial x_i}\left(\frac{\mu_t \partial k}{\sigma_k \partial x_i}\right) + P_k - \epsilon \tag{2}$$

$$\frac{\partial (U_i \epsilon)}{\partial x_i} = \frac{\partial}{\partial x_i}\left(\frac{\mu_t \partial \epsilon}{\sigma_\epsilon \partial x_i}\right) + c_{\epsilon_1}\frac{\varepsilon}{k}P_k - c_{\epsilon_2}\frac{\epsilon^2}{k} \tag{3}$$

where ρ is the air density, x_i are the position coordinates, p is the pressure, μ is the viscosity, and C_μ, C_{ϵ_1}, C_{ϵ_2}, σ_k, and σ_ϵ are the fixed constants for the $k-\epsilon$ model, with values set to 0.09, 1.55, 2.0, 1.0 and 1.3, respectively [28]. The two other terms are the turbulent viscosity, μ_t, given as

$$\mu_t = \frac{C_\mu k^2}{\epsilon} \tag{4}$$

and the turbulent production term, P_k, is given as

$$P_k = \mu_t\left(\frac{\partial U_i}{\partial x_j} + \frac{\partial U_j}{\partial x_i}\right)\frac{\partial U_i}{\partial x_j} \tag{5}$$

Near ground effects are not resolved within the CFD simulations. Instead, a roughness approximation is used in the log-law correlations for the boundary layer adopted from Toren and Petersen [29]. In this method, the terrain data from the national land cover database is converted to a numerical value normalized from 0 to 1. This value is set to 1.0 for city regions, 0.8 for heavily forested areas, 0.1 - 0.2 for farmland or plains covered in shrubs and set to 0 for flat areas. The roughness of the northern and southern region is shown in Fig. 2(a) and 2(b), respectively. The site is mostly desert and sagebrush with small changes seen due to clustered buildings and the highways.

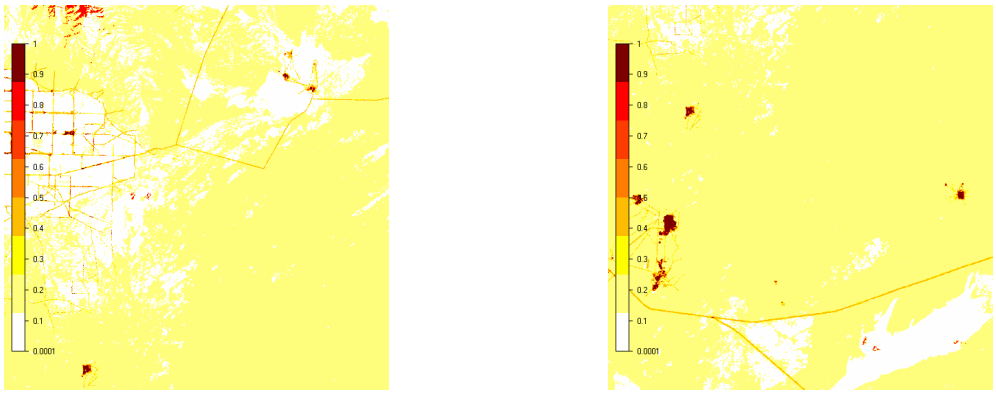

(a) (b)

Fig. 2. Roughness of the northern (left) and southern (right) domain of the INL site normalized from 0 to 1.

3.1 RESULTING CFD FLOW FIELD SIMULATIONS

There is a total of 12 CFD simulations, one for every 30-degrees of incoming wind direction. For the application of ampacity of transmission lines, only the near-ground wind at a height of 10 meters above ground is of interest. The wind field results at incoming wind direction of 0, 90, 180, and 270 degrees (left to right) is shown for the northern domain in Fig. 3. These results show significant changes in the wind field by the mountain range in the northwest corner, especially with regard to the northern and southern incoming wind flows. The southern region (not shown) has no mountains and shows very little changes in wind field patterns, except for the south-eastern edge. This corner of the terrain contains two high buttes which impact the wind flow.

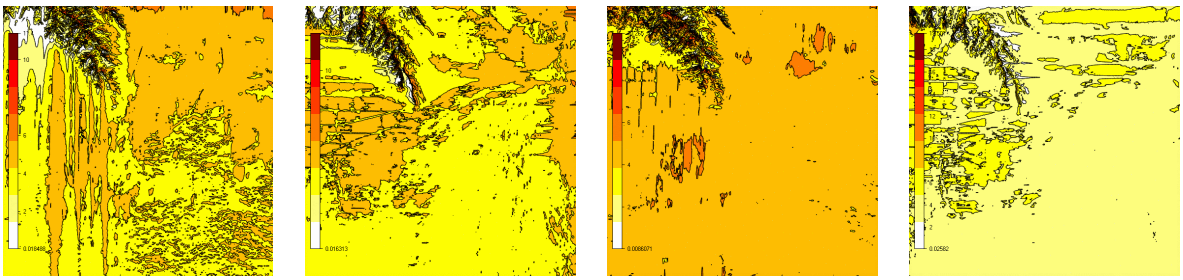

Fig. 3. Wind speed for the northern domain at 10 meters above the surface for incoming wind angles of 0, 90, 180, and 270 degrees, from left to right, respectively.

4. CONDUCTOR AMPACITY CALCULATIONS

It is common practice to calculate the ampacity of conductor is using the IEEE Standard 738, method for Calculating Current-Temperature Relationship of Bare Overhead Line Conductors [3]. The steady state current capacity is based on the heat balance equation. For overhead conductors it is given as

$$I = \sqrt{\frac{q_c + q_r - q_s}{R(T_c)}} \tag{6}$$

where q_s, q_r, and q_c are the heating though solar radiation, the radiation cooling, and the cooling through convection, respectively. The resistance of the line, R, is a function of the conductor temperature, T_c. It is assumed that radial temperature differences in the conductor are minor, thus the conductor temperature is the same as the line's surface temperature. The radiated heat loss rate per unit length of the transmission line is calculated as follows

$$q_r = 17.8 D \epsilon_c \left[\left(\frac{T_c + 273.15}{100} \right)^4 - \left(\frac{T_a + 273.15}{100} \right)^4 \right] \tag{7}$$

where ϵ_c is the conductor emissivity, D is the diameter of the conductor, and T_a is the ambient air temperature. The heat gain from the sun through solar irradiance is calculated by

$$q_s = \alpha Q_{se} \sin(\theta) A' \tag{8}$$

where α is the solar absorptivity, Q_{se} is the total solar radiated heat flux corrected by elevation, θ is the effective angle of incidence of the sun, and A' is the projected area of conductor per-unit length. The convective heat loss per unit length, q_c, is calculated using the maximum value of the following three convective equations based on the air speed. First, the natural convective heat loss rate given by

$$q_{cn} = 3.645 \rho_f^{0.5} D^{0.75} (T_c - T_a)^{1.25} \tag{9}$$

for low air speed, under 1.34 m/s, the term is given by

$$q_{c_1} = \left[1.01 + 1.35 \left(\frac{D V_w \rho_f}{u_f}\right)^{0.52}\right] k_f K_{angle} (T_c - T_a) \tag{10}$$

and for higher air speed the convective heat loss is given as

$$q_{c_2} = 0.754 \left(\frac{D V_w \rho_f}{\mu_f}\right)^{0.6} k_f K_{angle} (T_c - T_a) \tag{11}$$

where V_w is the speed of the air, K_{angle} is the wind direction factor, and the fluid parameters density, ρ_f, viscosity, μ_f, and thermal conductivity, k_f, are calculated at the film temperature, give as

$$T_f = \frac{T_c + T_a}{2} \tag{12}$$

Due to the high variability of the terrain, the air density is calculated as a function of elevation as well, as the parameter can vary as much as 20% over the entire transmission line segment. The wind direction factor is based on the angle between the wind direction and the conductor azimuth for each midpoint segment as

$$K_{angle} = 1.194 - \cos(\phi) + 0.194 \cos(2\phi) + 0.368 \sin(2\phi) \tag{13}$$

where ϕ is the angle of incidence between the wind direction and the midpoint azimuth with a maximum value of 90 degrees.

5. AMPACITY RATINGS VS. NUMBER OF HRRR MODEL POINTS

We evaluate the resulting ampacity rating based on the number of HRRR model points along the path of the transmission. The HRRR model points are used to represent an installation of a weather station. We use HRRR points because there are not enough weather stations along the path of the transmission lines studied. This method has been shown to produce accurate ampacity ratings when coupled with CFD simulation [13]. Five different scenarios, using 4, 10, 17, 26, and 35 model points along the transmission lines, are considered and shown in Fig. 5. Then number of model points relates to physical spacing between HRRR points of approximately 25, 10, 6, 4, and 3 km, respectively.

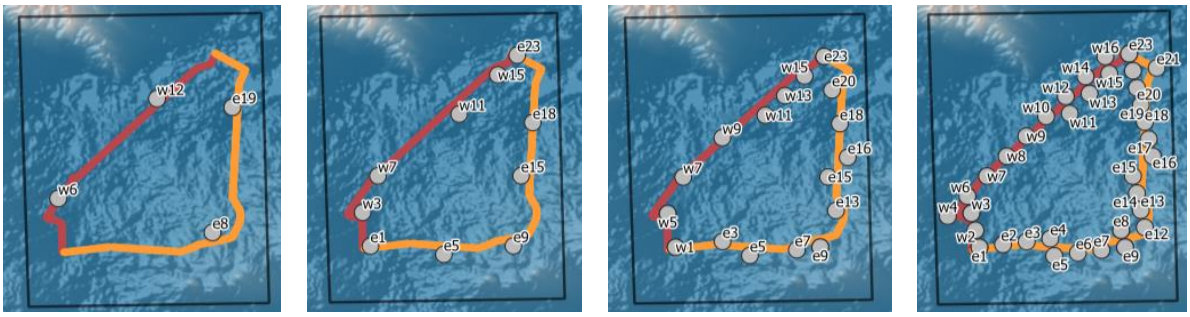

Fig. 4. The location of the HRRR model points used along the transmission lines under different scenarios.

The transmission lines studied use the same conductor over the entire path, so the limiting ampacity is only dependent on the environmental conditions. The ampacity for the two transmission lines is calculated along every span, and the limiting midpoint is used to determine the ampacity for the entire line. The data is analyzed for two full years from January 2018 through December 2019 for the 3-hour ahead HRRR forecast. The timeseries ampacity results are shown in Fig. 5(a) and 6(a) for the east and west loop, respectively. In these figures, an enlarged section showing the ampacity clearer over a week-long period is shown in (b). The immediate finding from the results is that the DLR ampacity oscillates between 400 and 900 amps, with an average higher in the winter months than the summer. In addition, the DLR rating is often above the SLR, and can be seen in the sorted values from largest to smallest shown in (c). The DLR is above the SLR roughly 97% of the time, i.e., the lines are underutilized during these times. However, it is just as important to note that there are times where near worst-case conditions occur. During these times if the lines were operated at the SLR ampacity, the lines could be overheated, potentially violating sag limitations or damaging equipment. However, further temporal analysis of the heating rates would be needed to evaluate this.

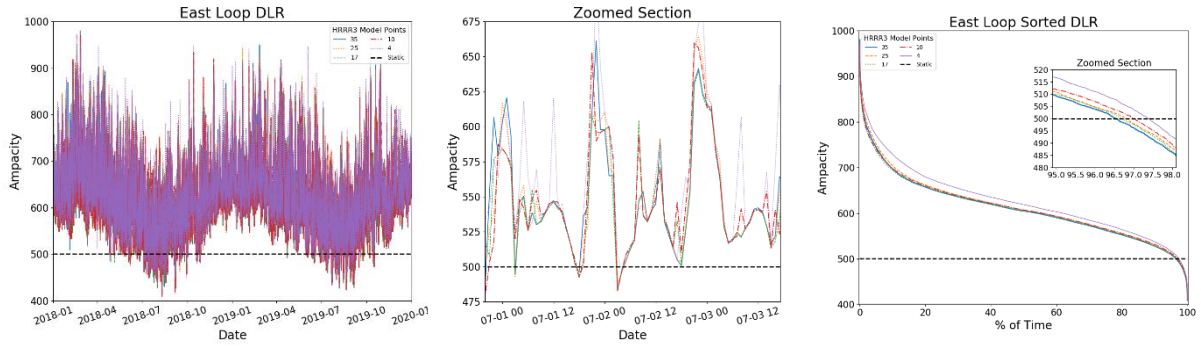

(a) (b) (c)

Fig. 5. The timeseries ampacity ratings of the east loop based on number of model points used over a 2-year period is shown in (a) with an enlarged view over a week in (b). Figure (c) shows the ampacity values sorted and highlights the amount of time that DLR exceeds SLR.

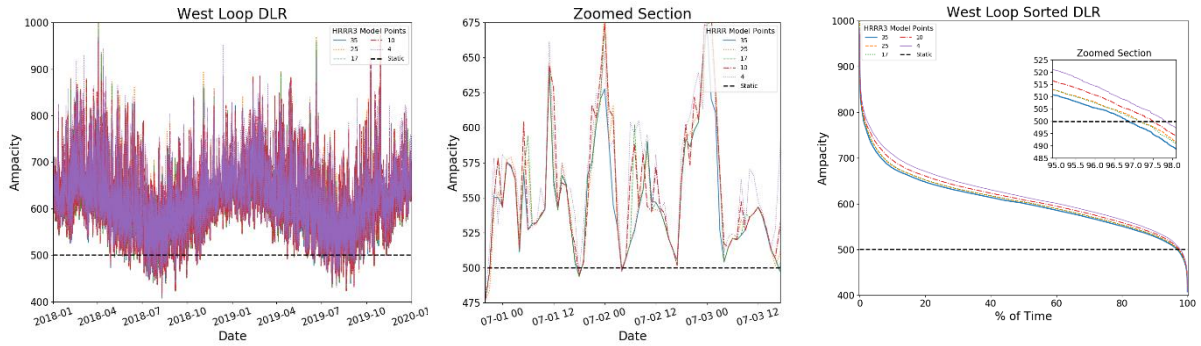

(a) (b) (c)

Fig. 6. The timeseries ampacity ratings of the west loop based on number of model points used over a 2-year period is shown in (a) with an enlarged view over a week in (b). Figure (c) shows the ampacity values sorted and highlights the amount of time that DLR exceeds SLR.

To evaluate the effects of spatial variation of HRRR model points on DLR ampacity ratings, the results of the timeseries plots must be observed. Here, a key finding is that additions of HRRR points result in decreased ampacity. However, the rate at which the ampacity profile decreases tends to reduce as the HRRR points are increased. It can be argued that this would indicate that the addition of more model points would not give different results. Thus, installing costly weather stations beyond that point would be unnecessary. To give a quantifiable value, we use the Root Mean Squared Error (RMSE), using the 35 model points as the true solution. The RMSE is given mathematically as

$$RMSE = \sqrt{\sum_{i=1}^{n} \frac{(x_i - y_i)^2}{n}} \tag{14}$$

Where x_i, y_i, and n are the predicted ampacity, the actual ampacity, and the number of data points, respectively. The RMSE results are given for the east and west loop in Table 1. Here, the amount of time DLR is greater than SLR is also given. Again, these results show that the ampacity of the lines has little change moving beyond 17 model points.

Table 1. Percent of time the DLR ampacity is greater than the static ampacity and the RMSE of each loop evaluated with different number of HRRR model points.

		East Loop		West Loop	
HRRR Model Points	Spacing (km)	DLR > SLR (% of time)	RMSE	DLR > SLR (% of time)	RMSE
4	25	97.4	39.9	97.8	38.9
10	10	97.0	27.5	97.5	26.0
17	6	96.7	19.1	97.1	14.5
26	4	96.8	16.1	97.1	14.0
35	3	96.5	-	96.9	-

6. CONCLUSION

In this work, we present a case study to demonstrate coupled DLR ampacity results with CFD simulations' flow fields. The resulting ampacity is based on spatial resolution of weather stations along the path of two transmission lines. The region in this studied lies in south eastern Idaho and is 30x50 km in size. There are two transmission lines across the region, we evaluate their ampacity over a 2-year period using 4, 10, 17, 26, and 35 HRRR model points along their path to represent weather stations at different spatial resolution. The results of this study indicate that increasing the density of weather stations decreases the ampacity ratings of the transmission lines. However, it is demonstrated that the decrease in ampacity diminish as additional points are added and converges to an ampacity rating that is independent of the number of weather stations. Thus, from an economic standpoint the cost/benefit of further addition of weather stations diminishes are more stations are added. These findings are intended to help transmission line operators evaluate the accuracy needed to safely operate their lines and the number of weather stations that would be required for implementing DLR.

7. ACKNOWLEDGMENT

This research was performed by Idaho National Laboratory (INL) with funding from the U.S. Department of Energy Wind Energy Technologies Office. INL is operated by Battelle Energy Alliance under contract No. DE-AC07-05ID14517.

BIBLIOGRAPHY

[1] CIGRE Technical Brochure 601, "Guide for thermal rating calculations of overhead lines," CIGRE working group B2.43, 2014

[2] IEC Standard TR 1597, "Overhead electrical conductors – calculation methods for stranded bare conductors," 1985

[3] IEEE Standard 738, "Standard for calculating current-temperature relationship of bare overhead line conductors," 2012

[4] IEEE PES Working Group Subcommittee 15.11, "Real-time overhead transmission line monitoring for dynamic rating," IEEE Transaction on Power Delivery. Vol. 31, num. 3, 2016

[5] J. Gentle, "Concurrent wind cooling in power transmission lines," Western Energy Policy research conference, Boise, ID. 2012

[6] D. Greenwood and P. Taylor, "Investing the impact of real-time thermal ratings on power network reliability," IEEE Transaction on Power Systems. vol. 23, no. 5, pp. 2460-2468, 2014

[7] J. Jiang, Y. Liang, C. Chen, X. Zheng, C. Chuang, and C. Wang, "On dispatching line ampacities of power grids using weather-based conductor temperature forecasts," IEEE Transaction on Smart Grid, vol. 9, no. 1, 2018

[8] T. Phillips, I. Senocak, J. Gentle, K. Myers, and P. Anderson, "Investigation of a dynamic power line rating concept for improved wind energy integration over complex terrain," ASME 2014 Joint US-European Fluids Engineering division summer meeting, 2014

[9] D. Greenwood, J. Gentle, K. Myers, P. Davison, I. West, J. Bush, G. Ingram, and M. Troffaes, "A comparison of real-time thermal rating systems in the U.S. and the U.K.," IEEE Transaction on Power Delivery, vol. 29, no. 4, pp. 1849-1858, 2014

[10] B. Bhattarai, J. Gentle, P. Hill, T. McJunkin, K. Myers, A. Abboud, R. Renwick, and D. Hengst, "Transmission line ampacity improvements of AltaLink wind plant overhead tie-lines using weather-based dynamic line ratings," IEEE PES General Meeting, 2017

[11] B. Bhattarai, J. Gentle, T. McJunkin, P. Hill, K. Myers, A. Abboud, and D. Hengst, "Improvement of transmission line ampacity utilization by weather-based dynamic line ratings," IEEE Transaction on Power Delivery, vol. 33, 2018

[12] B. Aznarte and N. Siebert, "Dynamic line rating using numerical weather predictions and machine learning: A case study," IEEE Transaction on Power Delivery, vol. 32, no. 1, pp. 335-343, 2017

[13] A. Abboud, K. Fenton, J. Lehmer, B. Fehringer, J. Gentle, T. McJunkin, K. Le Blanc, M. Petty, and M. Wandishin, "Coupling computational fluid dynamics with high resolution rapid refresh model for forecasting dynamic line ratings," Electric Power Systems Research, vol. 170, pp. 326-337, 2019

[14] A. Abboud, J. Gentle, T. McJunkin, and J. Lehmer, "Using computational fluid dynamics of wind simulations coupled with weather data to calculate dynamic line ratings," IEEE Transactions on Power Delivery, vol 35, no. 2, pp. 745-753, 2019

[15] C. Cong, P. Regulski, P. Wall, M. Osborne, and V. Terzija, "On the use of dynamic thermal-line ratings for improving operational tripping schemes," IEEE Transactions on Power Delivery, vol. 32, no. 4, pp. 1891-1900, 2016

[16] E. Qiu and J. Wang, "Distributionally robust congestion management with dynamic line rating," IEEE Transactions on Power Systems, vol. 30, no. 4, pp. 2198-2199, 2015

[17] L. Dawson and A. Knight, "Applicability of dynamic thermal line rating for long lines," IEEE Transactions on Power Delivery, vol. 33, no. 2, 2018

[18] "Dynamic line rating systems for transmission lines: American Recovery and Reinvestment Act of 2009," U.S. Department of Energy, 2014

[19] "Smart Grid System Report," U.S. Department of Energy, 2010

[20] High-Resolution Rapid Refresh (HRRR), https://rapidrefresh.noaa.gov/hrrr/

[21] Y.Yi, R. Harley, D. Divan, and T. Habetler, "Overhead conductor thermal dynamics identification by using echo state networks," International Joint Conference on Neural Network, pp. 3426-3443, 2009

[22] G. Bitsumalak, T. Stathopoulos, and C. Bedard, "Numerical evaluation of wind flow over complex terrain: review," Journal of Aero. Engineering, vol. 17, no. 4, pp. 135-145, 2004

[23] WindSim 9.0, https://windsim.com/software/windsim-10-0/windsim-9-0/

[24] T. Wallbank, “WindSim validation study: CFD validation in complex terrain,” 2018
[25] A. Dhunny, M. Lollchund, and S. Rughooputh, “Numerical analysis of wind flow patterns over complex hilly terrains: Comparison between two commonly used CFD software,” Int. J. Glob. Energy Issues, vol. 39, no. 3, pp. 181-203, 2016
[26] D. Greenwood, J. Gentle, K. Myers, P. Davison, I. West, J. Bush, G. Ingram, and M. Troffaes, “A comparison of real-time thermal rating systems in the U.S. and the U.K.,” IEEE Transaction on Power Delivery, vol. 29, no. 4, pp. 1849-1858, 2014
[27] T. Wallbank, “WindSim validation study: CFD validation in complex terrain,” WindSim, Tonsberg, Norway, 2008
[28] W. Jones and B. Launder, “The prediction of laminarization with a two-equation model of turbulence,” International Journal of Heat and Mass Transfer. vol. 15, no. 2, pp. 301-314, 1972
[29] I. Toren and E. Petersen, “European wind atlas,” Roskilde, Denmark, 1989